Published in final edited form as:
Methods. 2008 November ; 46(3): 213–223. doi:10.1016/j.ymeth.2008.09.024.

Calcium, mitochondria and apoptosis studied by fluorescence measurements

Soumya Sinha Roy and **György Hajnóczky***
Department of Pathology, Anatomy and Cell Biology, Thomas Jefferson University, 1020 Locust Street, Suite 253 JAH, Philadelphia, PA 19107, USA

Abstract

Among the many unsolved problems of calcium signalling, the role of calcium elevations in apoptotic and necrotic cell death has been a focus of research in recent years. Evidence has been presented that calcium oscillations can effectively trigger apoptosis under certain conditions and that dysregulation of calcium signalling is a common cause of cell death. These effects are regularly mediated through calcium signal propagation to the mitochondria and the ensuing mitochondrial membrane permeabilization and release of pro-apoptotic factors from mitochondria to the cytoplasm. The progress in this area depended on the development of (1) fluorescent/luminescent probes, including fluorescent proteins that can be genetically targeted to different intracellular locations and (2) the digital imaging technology, fluorescence-activated cell sorting and fluorescent high through put approaches, which allowed dynamic measurements of both $[Ca^{2+}]$ in the intracellular compartments of interest and the downstream processes. Fluorescence single cell imaging has been the only possible approach to resolve the cell-to-cell heterogeneity and the complex subcellular spatiotemporal organization of the cytoplasmic and mitochondrial calcium signals and downstream events. We outline here fluorometric and fluorescence imaging protocols that we set up for the study of calcium in the context of apoptosis.

Keywords

Calcium; Mitochondria; ER; Apoptosis; Wave; ROS; Cytochrome *c*; Caspase

1. Introduction

The extracellular Ca^{2+} concentration is >1 mM, whereas the cytoplasmic Ca^{2+} concentration ($[Ca^{2+}]_c$) is ≈100 nM at the resting state. $[Ca^{2+}]$ in the mitochondrial matrix ($[Ca^{2+}]_m$) and nuclear matrix is similar to $[Ca^{2+}]_c$. By contrast, the endoplasmic reticulum (ER) (sarcoplasmic reticulum (SR) in muscle cells) shows high Ca^{2+} concentration (100–500 μM) as compared to $[Ca^{2+}]_c$. The activity of the plasma membrane Ca^{2+} pumps (PMCA) and the sarco/endoplasmic reticulum Ca^{2+} ATPases (SERCAs) is primarily responsible for the maintenance of the large $[Ca^{2+}]$ gradients. Opening of the ER/SR Ca^{2+} release channels, IP_3 receptors (IP3Rs) and ryanodine receptors (RyRs) results in Ca^{2+} mobilization from the ER/SR that manifests as a decrease of $[Ca^{2+}]_{ER}$ and an increase of $[Ca^{2+}]_c$ [1]. Activation of plasma membrane Ca^{2+} channels allows Ca^{2+} to enter along the concentration and electrical gradients and also yields a $[Ca^{2+}]_c$ increase. The mitochondrial matrix is separated from the cytoplasm by two membranes and the inner mitochondrial membrane (IMM) has a very limited permeability to ions. However, conditions of elevated $[Ca^{2+}]_c$ evoke activation of

*Corresponding author. Fax: +1 215 923 2218. Gyorgy.Hajnoczky@jefferson.edu (G. Hajnóczky).

the Ca^{2+} uniporter that mediates $\Delta\Psi_m$-driven Ca^{2+} uptake to the mitochondria [2,3]. Despite the presence of robust Ca^{2+} buffering capacity in the mitochondrial matrix, $[Ca^{2+}]_c$ spikes yield rapid elevations in $[Ca^{2+}]_m$ from 100 nM to at least micromoclar and in some cases over hundred micromolar [4]. Due to the relatively low affinity of the uniporter, the global $[Ca^{2+}]_c$ rise (≈1 μM) established by ER C a^{2+} release and Ca^{2+} entry during physiological $[Ca^{2+}]_c$ signals results in only a slow increase in $[Ca^{2+}]_m$. However, long-lasting global $[Ca^{2+}]_c$ signals may result in accumulation of vast amounts of Ca^{2+} in the mitochondria. Alternatively, mitochondria close to the ER or plasma membrane may sense the large and local $[Ca^{2+}]_c$ increases in proximity to the activated Ca^{2+} channels and exhibit a $[Ca^{2+}]_m$ rise closely coupled to the rise of the $[Ca^{2+}]_c$ signal [5].

In physiological conditions, calcium signal propagatin to the mitochondria results in stimulation of ATP production through activation of the Ca^{2+}-sensitive dehydrogenases and yields feed back effects on cytoplasmic calcium signalling (Fig. 1A). However, Ca^{2+} overloading of the mitochondria triggers permeability transition pore (PTP) opening that appears as uncoupling, IMM reorganization, mitochondrial swelling and finally, outer mitochondrial membrane (OMM) permeabilization [6–9]. Disruption of the OMM barrier induces apoptosis by stimulating the release of apoptosis promoting factors from the mitochondrial intermembrane space (IMS) to the cytoplasm (cyto *c*, AIF, Smac/DIABLO, OMI/HtrA2, pro-caspases, etc.) and by impairing mitochondrial function [10,11]. The PTP is thought to be a multi-protein complex that is assembled at the contact sites between the IMM and OMM but the exact molecular composition of the PTP has not been elucidated [12]. In the presence of various stress factors (e.g. ceramide, arachidonic acid, reactive oxygen species (ROS) etc.) the PTP becomes sensitized to physiological $[Ca^{2+}]_m$ spikes that in turn, trigger mitochondrial membrane permeabilization and apoptosis instead of a metabolic response (Fig. 1B) [13–17]. Alternatively, conditions that enhance the Ca^{2+} mobilizatin from the ER/SR or recruit massive Ca^{2+} entry may augment the mitochondrial Ca^{2+} uptake to cause alone activation of the PTP and apoptosis (Fig. 1C) [18]. These conditions may include mutations in the IP3R/RyR or in their associated proteins (e.g. huntingtin) [19], posttranslational modifications of IP3R/RyR and pathologic activation of the NMDA receptors by glutamate, glutamate excitotoxicity [20]. Furthermore, narrowing the ER-mitochondrial gap by synthetic interorganellar linkers also causes increased Ca^{2+} transfer to the mitochondria and promotes mitochondrial overload and apoptosis [21]. Another remarkable feature of the activation of PTP by Ca^{2+} is that the opening of the PTP permits release of the accumulated Ca^{2+} that is subsequently taken up by adjacent mitochondria (Fig. 1C). This mechanism may result in a regenerative response that spreads throughout the entire mitochondrial population of the cell as a propagated wave [22,23]. Notably, mitochondrial Ca^{2+} may also recruit ROS formation and ROS formation and release from the mitochondria can also form a regenerative mechanism for driving mitochondrial waves [24,25]. PTP-dependent intermitochondrial calcium signaling has been reported to recruit mitochondria to the apoptotic process [26]. As a high density of mitochondria facilitates communication between neighboring organelles, the local signalling machinery can be utilized effectively in the large myotubes of heart and skeletal muscle that are among the cells most abundant in mitochondria. Thus, the calcium signal→ $[Ca^{2+}]_m$ rise→ PTP opening→OMM permeabilization axis effiently triggers the execution of apoptosis and is likely to be relevant in tissue damage under a variety of stress conditions and genetic alterations.

This review describes experimental approaches that can be used for analysis of the role of calcium signalling in apoptosis. These methods target primarily the mitochondrial phase of apoptosis. Direct measurements of $[Ca^{2+}]_c$ and $[Ca^{2+}]_m$ in both intact and permeabilized cells became feasible using Ca^{2+} sensitive fluorophores and florescent proteins. Monitoring of the $\Delta\Psi_m$ allows detection of the PTP opening and can be conducted using potentiometric

dyes. Cytochrome *c* release from the mitochondria can be assessed by monitoring the distribution of cytochrome *c*-GFP (cyto *c*-GFP) between mitochondria and cytosol. Caspase activation, phosphatidylserine (PS) exposure and nuclear apoptosis can also be monitored using florescent probes. Application of these probes in fluorometry or in fluorescence imaging allows dynamic measurements of the respective parameters in real-time. Furthermore, fluorescence imaging also offers resolution of the individual cell responses and the intracellular spatiotemporal pattern of the measured parameters. Combination of these capabilities is extremely valuable for the study of calcium signalling in apoptosis and is a distinctive feature of fluorescence imaging. However, other approaches like luminescence measurements of genetically targeted reporters (e.g. Ca^{2+} and ATP) [27] and fluorescence activated cell sorting [28] have their own edge and provide complementary information.

2. Methods

2.1. Cells and reagents

Cell Culture—

1. Human hepatoma cell line HepG2 (ATCC) and rat cardiac muscle cell line H9c2 (ATCC).
2. Dulbecco's Modified Essential Medium (DMEM) supplemented with 10% fetal bovine serum (Gibco), 1 mM Sodium Pyruvate (Gibco), 2 mM L-glutamine (Biowhittaker), 100 U/ml Penicillin and 100 μg/ml Streptomycin (Biowhittaker).
3. Solution of Trypsin (0.25%) and EDTA (1 mM) (Gibco).
4. Poly-D-lysine-coated 25 mm round glass coverslips.
5. Cyto *c*-GFP expressing cells were generated by transfection using plasmid DNA [29] and Lipofecta-AMINE 2000 (Invitrogen) [26].
6. For the studies with myotubes H9c2 cells were grown to reach confluency (1 week on average) and subsequently for an additional 3–7 days to allow differentiation [30].

Assay Buffers—

1. Extracellular medium with 2% bovine serum albumin (BSA) (2% BSA/ECM) consisting of 121 mM NaCl, 5 mM $NaHCO_3$, 10 mM Na–Hepes, 4.7 mM KCl, 1.2 mM KH_2PO_4, 1.2 mM $MgSO_4$, 2 mM $CaCl_2$ and 10 mM glucose, pH 7.4.
2. Extracellular medium with 0.25% BSA (0.25% BSA/ECM) consisting of 121 mM NaCl, 5 mM $NaHCO_3$, 10 mM Na–Hepes, 4.7 mM KCl, 1.2 mM KH_2PO_4, 1.2 mM $MgSO_4$, 2 mM $CaCl_2$ and 10 mM glucose (BSA), pH 7.4.
3. Ca^{2+} free extracellular buffer (Na–Hepes–EGTA), containing 120 mM NaCl, 5 mM KCl, 1 mM KH_2PO_4, 0.2 mM $MgCl_2$, 0.1 mM EGTA, 20 mM Hepes–NaOH pH 7.4.
4. Intracellular medium (ICM) composed of 120 mM KCl, 10 mM NaCl, 1 mM KH_2PO_4, 5% Dextran, 20 mM Hepes–Tris pH 7.2 supplemented with 1 μ/ml of each of antipain, leupeptin and pepstatin (Sigma). To lower the ambient $[Ca^{2+}]$, the ICM was passed through a Chelex 100 column (Bio-Rad) prior to addition of protease inhibitors to lower the ambient $[Ca^{2+}]$.

Fluorophores—To monitor $[Ca^{2+}]_c$, $[Ca^{2+}]_m$ and $\Delta\Psi_m$ in both intact and permeabilized cells and to visualize cytochrome *c*, annexin distribution, effector caspase activation and

nuclear morphology the following fluorophores and excitation and emission wave lengths were used (Table 1). All fluorophores were obtained from Molecular Probes except where it is indicated otherwise.

2.2. Instrumentation

Fluorescence measurements were conducted in suspensions of cells and in single cells using the approaches and instruments listed in Table 2. In single cell imaging experiments, images were captured using 40× UApo and 60× PlanApo objectives at Olympus IX70 and 81 inverted microscopes.

2.3. Experimental protocols

2.3.1. Fluorometric measurement of $[Ca^{2+}]_c$ and $\Delta\Psi_m$ in suspensions of permeabilized cells—Cells harvested using 0.25% trypsin–EDTA were washed in ice cold Na–Hepes–EGTA. Equal aliquots of cells (2.4 mg protein) were resuspended in 1.5 ml of ICM and permeabilized with 30–40 μg/ml digitonin in a plastic cuvette (Sarstedt) under magnetic stirring at 37°C. All the measurements were carried out in the presence of 2 mM MgATP and an ATP regenerating system composed of 5 mM phosphocreatine, 5 U/ml creatine kinase. Mitochondria were energized with 2 mM succinate (complex II substrate) or with 1 mM malate/5 mM glutamate (complex I substrate). To carry out simultaneous measurements of $[Ca^{2+}]_c$ and ΔW_m, the permeabilized cells were supplemented with 0.5 μM fura2FF/FA and 800 nM JC-1 or 2 μM TMRE and fluorescence measurements were done in a multi-wave length-excitation dual wave length-emission fluorometer (see Table 2) using respective excitations and emissions for the above dyes (Table 1). The relatively low affinity of fura2FF for Ca^{2+} (K_d ~4 μM) was favorable for avoiding saturation of the dye during large increases of $[Ca^{2+}]_c$. After reaching a steady-state in $\Delta\Psi_m$, 3 pulses of $CaCl_2$ (30–50 μM each) were added in the cuvette by a Hamilton syringe during continuous recording. The amount of added $CaCl_2$ was chosen so that the last pulse evoked a reversible depolarization and $[Ca^{2+}]_c$ rise gradually recovering in 2–3 min in the control cells. However, when the PTP's sensitivity towards Ca^{2+} was increased, depolarization become prolonged and the recovery of $[Ca^{2+}]_c$ was delayed or turned to a progressive increase (delayed Ca^{2+} dysregulation). Stress agents like C2-ceramide (C2), dihydro-C2-ceramide (negative control) (Alexis) (40 μM) or H_2O_2 (50–200 μM) (Sigma), which were applied for sensitization of the Ca^{2+}-induced activation of the PTP were added 180 s prior to the Ca^{2+} pulsing. Cyclosporin A (CsA, 2 μM), an inhibitor of the PTP, was added from the start of the recording to clarify the involvement of PTP in the stress agent and Ca^{2+}-induced changes in $\Delta\Psi_m$ and $[Ca^{2+}]_c$. In most measurements, thapsigargin (Tg), an inhibitor of the SERCA Ca^{2+} pump (2 μM) was included to abolish the ER Ca^{2+} uptake so the added Ca^{2+} was accumulated only by the mitochondria. Calibration of the furaFF signal was carried out at the end of each measurement by adding 1.5 mM $CaCl_2$ and subsequently 10 mM EGTA–Tris pH 8.5. The K_d of fura2FF for Ca^{2+} (4 μM) was determined using a $[Ca^{2+}]$ calibration buffer series ranging from 65 nM to 10 mM (Calcium Calibration Kits #2&3; Molecular Probes). $[Ca^{2+}]_c$ was calculated by using a K_d of 4 uM [31]. At the end of the fluorescent measurement of $\Delta\Psi_m$ and $[Ca^{2+}]_c$, membrane and cytosolic fractions were separated rapidly by centrifugation for 5 min at 12000 rpm. Membrane fractions contained the mitochondria; whereas soluble factors (e.g. pro-apoptotic proteins) exited the mitochondria were recovered in the cytosolic fractions. Cytosolic and membrane fractions were used to assess the distribution of cytochrome *c*, AIF, Smac/DIABLO, OMI/HtrA2 and pro-caspases and to quantitate caspase-3 activity.

2.3.2. Imaging of $[Ca^{2+}]_c$[$Ca^{2+}]_m$ and $\Delta\Psi_m$ in permeabilized individual cells—Cells grown in coverslips were loaded with 4 μM rhod2/AM or rhod2FF/AM in 2% BSA/ECM in the presence of 0.003% (w/v) pluronic acid at 37 °C for 50 min or with 25–80 nM

TMRE for 15 min. TMRE (2.5–10 nM) was also present in the medium during the measurements. Dye-loaded cells were washed with a Na–Hepes–EGTA and then permeabilized by incubation for 5 min with 15–25 μg/ml digitonin in ICM. In most of the experiments, 10–20 μM EGTA was also present during permeabilization to maintain $[Ca^{2+}]$ at 20–50 nM. After permeabilization, the cells were washed into fresh ICM with out digitonin and incubated in the imaging chamber at 35°C. All the measurements were carried out in the presence of 2 mM MgATP and ATP regenerating system composed of 5 mM phosphocreatine, 5 U/ml creatine kinase. Mitochondria were energized with 2 mM succinate or 1 mM malate/5 mM glutamate. In some experiments 2.5 μg/ml oligomycin was also added to prevent reversed function of the mitochondrial H^+ ATPase. Medium free $[Ca^{2+}]$ was <100 nM after Chelex treatment and did not exceed 250–350 nM after addition of protease inhibitors, ATP and mitochondrial substrates. To monitor $[Ca^{2+}]_c$, 5 μM fluo3FF (K_d ~16 μM) was added to the bathing medium after cell permeabilization. The bath volume was 1 ml. To make additions, 200–300 μl of medium were taken out, mixed with the stimulus, returned to the chamber and resuspended with two strokes. Permeabilized cells were exposed to 40 μM C2 for 5 min prior to addition of Ca^{2+} and C2 was also present during the entire experiments. Fluorescence recording was carried out using either an epifluorescence or a confocal imaging system described in Table 2 using the excitation and emission wavelengths listed in Table 1. In most cases, simultaneous recording of $[Ca^{2+}]_c$ and $[Ca^{2+}]_m$ or $[Ca^{2+}]_c$ and $\Delta\Psi_m$ was performed. Images were collected every 2–6 s. To quantitate responses of individual cells, whole cell areas were masked, whereas to evaluate time courses at subcellular resolution, intracellular regions (30–50 pixels each) were selected along the path of wave propagation. Wave rates were calculated by measuring the time offset in either the falling phase of $\Delta\Psi_m$ or in the rising phase of $[Ca^{2+}]_c$ or $[Ca^{2+}]_m$ or at half-peak height over known distances within individual myotubes.

2.3.3. Imaging of $[Ca^{2+}]_c\Delta\Psi_m$, cytochrome c distribution and caspase activation in intact single cells—

For measurements of $[Ca^{2+}]_c$ and $\Delta\Psi_m$ in intact cells, the cells were pretreated with 40 μM C2 for 2–5 h prior to stimulation by a Ca^{2+}-mobilizing agonist (caffeine, ATP or Tg). Cells grown in coverslips were loaded with 5 μM fluo3/AM and 25–50 nM TMRE in 2% BSA ECM in the presence of 0.003% (w/v) pluronic acid and 200 μM sulfinpyrazone at room temperature for 25 and 15 min, respectively. Sulfnpyrazone was also present during the imaging measurements to minimize dye loss. Experiments were performed in 0.25% BSA/ECM at 35 °C. To visualize cytochrome *c* release from the mitochondria, cyto *c*-GFP transfected cells were used. To measure caspase-3(-like) activity, the TMRE-loaded cells were incubated with 5–10 μM fluorogenic caspase-3 substrate (PhiPhiLux-G_1D_2). Imaging experiments were performed in RPMI. To quantitate changes in PhiPhiLux fluorescence, the image series was background subtracted and total cell areas or intracellular regions were masked. To evaluate PS exposure, the cells were labeled with annexin–Alexa Fluor 488 according to the manufacturer's instructions. In order to visualize apoptotic and necrotic cells, labeling of the cells with 10 μg/ml Hoechst 33342 for 5 min was carried out and 1 μg/ml propidium iodide was present during fluorescence imaging. All the imaging experiments were carried out using either an epifluorescence or a confocal imaging system described in Table 2. Excitation wave lengths used for the above mentioned probes are listed in Table 1.

2.4. A word of caution

Cell permeabilization—To achieve permeabilization of the plasma membrane in >99% of the cells and to avoid permeabilization of the mitochondrial and ER membranes the digitonin concentration has to be individually titrated for each cell type. To determine the lowest effective concentration of digitonin we used Trypan Blue that only enters the cells

upon the loss of the plasma membrane barrier and visualized the blue permeabilized cells under a microscope.

Dye loading—Dye concentrations and the conditions for dye loading vary between different cell types. So it is important to optimize dye loading condition (e.g. concentration of dye, duration and temperature of loading) for each cell type.

Cell contraction and movement—In many myotubes, the Ca^{2+} signal was associated with cell contraction. To make sure that the fluorescence changes were not due to cell contraction, we checked the position of the cells at the beginning as well as at the end of every imaging measurement. Furthermore, in most experiments, two fluorophores were monitored simultaneously, and by evaluation of both signals we could determine the position of the myotubes throughout the experiments.

Illumination intensity—Excitation light should be kept at the lowest intensity that is sufficient for the cell analysis. It is practical to use a dichroic reflector, an emission filter and a detector, which allow efficient detection of the emitted light so less excitation is needed. High illumination intensity, in particular the laser light causes photobleaching and ROS generation promoting cell death.

3. Examples of measurements

3.1. Fluorometric evaluation of the PTP-dependent $[Ca^{2+}]_c$ dysregulation in permeabilized cells

Various pro-apoptotic agents (C2, H_2O_2, arachidonic acid, ethanol, staurosporine etc.) have been found to sensitize the Ca^{2+}-induced opening of the mitochondrial PTP. The increase in IMM permeability causes dissipation of the $\Delta\Psi_m$ and prevents Ca^{2+} retention in the mitochondria. This can be easily detected by fluorometric measurement of $[Ca^{2+}]_c$ in suspensions of permeabilized cells exposed to Ca^{2+} pulsing. In Fig. 2 measurement of $[Ca^{2+}]_c$ was carried out in permeabilized HepG2 (left panel) and H9c2 (right panel) cells. Addition of Ca^{2+} pulses induced a rise in $[Ca^{2+}]_c$ that activated mitochondrial uptake of Ca^{2+} as evidenced by the falling phase of $[Ca^{2+}]_c$ signals. In naive cells mitochondrial Ca^{2+} uptake could bring down the $[Ca^{2+}]_c$ rise almost to the baseline. The cells pretreated with C2 or H_2O_2 handled the first Ca^{2+} pulse like the naive cells but the subsequent Ca^{2+} additions caused progressive loss of the mitochondrial Ca^{2+} uptake referred as delayed $[Ca^{2+}]_c$ dysregulation. An inverse correlation appears between the sensitization of the PTP towards Ca^{2+} and the amount of Ca^{2+} pulses effectively handled by the mitochondria. The involvement of the PTP in this process was confirmed by adding CsA together with the stress agents, which prevented the delayed $[Ca^{2+}]_c$ dysregulation (Fig. 2A). To demonstrate the mitochondrial depolarization and swelling caused by the PTP opening, fluorometric measurement of the $\Delta\Psi_m$ and light scattering can be performed simultaneously with the recording of $[Ca^{2+}]_c$.

3.2. Real-time imaging of the mitochondrial $[Ca^{2+}]$ signal, depolarization and cyto c-GFP release in permeabilized single cells

The experiment described under 3.1. showed Ca^{2+}-induced PTP opening in populations of several millions of permeabilized cells. However, individual cells display heterogeneity in both calcium signalling and apoptosis. Thus it is of significance to analyze in single cells the Ca^{2+} transfer to the mitochondria, PTP-opening and the ensuing OMM permeabilization. These processes can be assessed in individual cells by fluorescence imaging of $[Ca^{2+}]_c$, $[Ca^{2+}]_m$, $\Delta\Psi_m$ and cyto *c*-GFP distribution. Furthermore, these approaches also provide

information on the subcellular organization of the mitochondrial events produced by hundreds of discrete mitochondria in many cell types.

3.2.1. Simultaneous measurement of $[Ca^{2+}]_c$ and $[Ca^{2+}]_m$—Ca^{2+} transfer to the mitochondria and the PTP-dependent Ca^{2+} release was monitored with confocal imaging of $[Ca^{2+}]_c$ and $[Ca^{2+}]_m$ in permeabilized H9c2 myotubes. Myotubes were preincubated with Tg and Ryanodine (Ry) to eliminate the SR Ca^{2+} storage and were pretreated with C2 for sensitizing the Ca^{2+}-induced PTP opening. Addition of a $CaCl_2$ pulse (50 μM) to raise $[Ca^{2+}]_c$ from 250 nM to 15 μM evoked a rapid $[Ca^{2+}]_c$ rise followed by a $[Ca^{2+}]_m$ elevation throughout the cell at the same time. Due to the small amount of cells present in the imaging chamber mitochondrial Ca^{2+} uptake could not lower $[Ca^{2+}]_c$ to the resting level. Instead, 10 min after the onset of the mitochondrial Ca^{2+} uptake a second and robust elevation in $[Ca^{2+}]_c$ appeared. Importantly, in the absence of C2, addition of 50 μM $CaCl_2$ did not induce a delayed $[Ca^{2+}]_c$ increase in 20 min [26]. Since the SR Ca^{2+} transport was inhibited, Ca^{2+} release from the mitochondria was the likely source of the delayed $[Ca^{2+}]_c$ elevation. Indeed, CsA pretreatment abolished the delayed Ca^{2+} increase [26]. The PTP-mediated mitochondrial Ca^{2+} release did not appear as a $[Ca^{2+}]_m$ decrease but when the mitochondrial Ca^{2+} tracer, rhod2 was replaced with a lower affinity probe, rhod2FF a decay in $[Ca^{2+}]_m$ preceding the delayed $[Ca^{2+}]_c$ rise could be visualized [26]. Evaluation of a large number of cells using the protocol shown in Fig. 3A revealed cell-to-cell heterogeneity in the lag time of the delayed $[Ca^{2+}]_c$ dysregulation but always led to discharge of the entire population of mitochondria. Furthermore, the time-lapse images revealed that the delayed $[Ca^{2+}]_c$ dysregulation appeared as a $[Ca^{2+}]_c$ wave slowly propagating through the entire cell (Fig. 3A). Since velocity of the wave and rate of $[Ca^{2+}]_c$ rise do not decline with distance from the site of wave origin, a regenerative model that includes signaling between neigh boring mitochondria may underlie the observed kinetics of the delayed $[Ca^{2+}]_c$ waves. Cell to cell heterogeneity was noticed in regard to the location of the initiation site and the velocity of wave propagation, which seem to depend on the intrinsic properties of the mitochondrial uptake sites and the increase in mitochondrial excitability evoked by the PTP-sensitizing agents [26].

3.2.2. Simultaneous measurement of $[Ca^{2+}]_c$ and $\Delta\Psi_m$—Dissipation of the $\Delta\Psi_m$ is a direct consequence and a frequently used marker of the PTP opening. To further study the mechanism of the delayed mitochondrial Ca^{2+} release waves, confocal imaging of $\Delta\Psi_m$ simultaneously with $[Ca^{2+}]_c$ was performed in C2-pretreated permeabilized myotubes (Fig. 3B). Addition of Ca^{2+} was followed by a wave of mitochondrial depolarization that was coupled to the wave of the delayed $[Ca^{2+}]_c$ elevation. When a Ca^{2+} chelator, EGTA was added, the evolution of $\Delta\Psi_m$ and $[Ca^{2+}]_c$ waves was interrupted and partial regeneration of $\Delta\Psi_m$ was observed. When the elevated global $[Ca^{2+}]_c$ was reestablished by addition of $CaCl_2$, the waves resumed and appeared to progress without change in direction. The waves were also halted by addition of ruthenium red (RuRed), an inhibitor of the mitochondrial Ca^{2+} uniporter. Thus, the $[Ca^{2+}]_c$ elevation wave and mitochondrial Ca^{2+} uptake appear to be essential for the wave propagation. If mitochondrial Ca^{2+} uptake occurs, elevation of $[Ca^{2+}]_m$ may result in PTP opening and Ca^{2+} release, which subsequently loads up the next group of mitochondria. This Ca^{2+} cycle may provide the regenerative mechanism underlying the PTP-dependent $[Ca^{2+}]_c$, $[Ca^{2+}]_m$ and $\Delta\Psi_m$ wave propagation. In the experiments shown above the ER/SR Ca^{2+} transport was inhibited to isolate the mechanism of the delayed $[Ca^{2+}]_c$ dysregulation and waves in the mitochondria. However, if the ER/SR Ca^{2+} stores were charged the IP3 R/RyR-mediated Ca^{2+} oscillations could also provide sufficient Ca^{2+} trigger to induce PTP opening in C2-pretreated cells [13,26].

3.2.3. Coupling of cyto c-GFP release to the PTP-dependent dissipation of the $\Delta\Psi_m$—An indispensable component of the mitochondrial phase of apoptosis is the release of proteins from the IMS that unmask their proapoptotic activity in the cytoplasm. Cytochrome *c* is the classical example for these proteins. To monitor the effect of the Ca^{2+}-induced PTP opening on cytochrome *c* release time-lapse fluorescence imaging was performed in permeabilized HepG2 cells transfected with cyto *c*-GFP and loaded with TMRE. Cyto *c*-GFP was colocalized with TMRE, indicating the mitochondrial localization of the fusion protein (Fig. 3C). Upon pretreatment with C2 and addition of Ca^{2+}, the TMRE fluorescence disappeared, indicating complete depolarization (Fig. 3C). Similar to the H9c2 myotubes, the Ca^{2+}-induced depolarization also appeared as a wave in HepG2 cells (Fig. 3C). The loss of $\Delta\Psi_m$ was followed by a gradual and partial decrease in cyto *c*-GFP fluorescence (Fig. 3C). This process could be prevented by CsA treatment (not shown). Finally, addition of tBid, a pro-apoptotic BH3 only protein that activates Bak/Bax to permeabilize the OMM, caused completion of the cyto *c* release (Fig. 3C). Thus, the combined effect of C2 and Ca^{2+} caused cytochrome *c* release that was dependent on PTP opening. C2 + Ca^{2+}-induced partial release of the native cytochrome *c* has also been documented by biochemical analysis and by immunocytochemistry.

3.3. Real-time imaging of the calcium signal driven depolarization, cyto c-GFP release and caspase activation in intact individual cells

Isolated organelles and permeabilized cells provide a straightforward model for the study of the Ca^{2+} or Ca^{2+} mobilization-dependent mitochondrial membrane permeabilization. However, initiation of a calcium signal by cell surface receptors and development of the complete apoptotic cascade requires intact cells. In addition to the calcium signal and mitochondrial permeabilization, time-lapse imaging of caspase activation and visualization of PS exposure and nuclear condensation/fragmentation is also feasible in intact cells.

3.3.1. Simultaneous measurement of $[Ca^{2+}]_c$ and $\Delta\Psi_m$ during RyR-mediated Ca^{2+} mobilization—Time-lapse confocal imaging of $[Ca^{2+}]_c$ and $\Delta\Psi_m$ was performed in C2 pretreated intact H9c2 myotubes. To rapidly mobilize the SR Ca^{2+} store, caffeine was added together with Tg. RyR-mediated Ca^{2+} mobilization appeared as a rapid and large initial increase in $[Ca^{2+}]_c$ followed by a plateau phase and by a late increase (Fig. 4A, lower left graph). During the plateau phase the effect of Ca^{2+} entry on $[Ca^{2+}]_c$ is balanced by continuous mitochondrial Ca^{2+} uptake. The image series in Fig. 4A shows that the late $[Ca^{2+}]_c$ rise propagated as a wave throughout the C2-pretreated cells. Furthermore, the late $[Ca^{2+}]_c$ increase wave was closely coupled to a wave of mitochondrial depolarization (Fig. 4A). The late response was prevented by CsA. Thus, the calcium signal brought about mitochondrial sequestration of Ca^{2+} and the ensuing $[Ca^{2+}]_m$ rise triggered mitochondrial depolarization and Ca^{2+} release waves that exhibit similar propagation properties to the waves recorded in permeabilized cells.

3.3.2. Simultaneous measurement of $[Ca^{2+}]_c$ and $\Delta\Psi_m$ during IP_3-linked Ca^{2+} mobilization—To determine whether calcium signals evoked by IP_3-linked agonists are able to initiate the mitochondrial phase of apoptosis in C2-treated intact cells, simultaneous fluorescence measurements of $\Delta\Psi_m$ and $[Ca^{2+}]_c$ were carried out in HepG2 cells by activation of the IP_3-linked calcium signaling pathway through P_{2y} receptors with ATP (Fig. 4B). Addition of ATP evoked rapid and transient rises of $[Ca^{2+}]_c$ in naive and C2-treated cells as well (increase of the green component in Fig. 4B, images iv and v). In C2-pretreated cells, ATP also induced substantial mitochondrial depolarization that was eliminated in the presence of CsA (Fig. 4B). These data illustrated that the calcium signal evoked by an IP_3-linked agonists led to opening of the PTP in C2-pretreated HepG2 cells but not in the control.

3.3.3. Visualization of cyto c-GFP release elicited by IP_3-induced Ca^{2+} mobilization—To test whether the Ca^{2+}-dependent PTP opening results in cytochrome *c* release in intact cells, confocal imaging was used to visualize intracellular distribution of cytochrome *c* in cyto *c*-GFP expressing HepG2 cells (Fig. 4C). Naive and C2 pretreated intact HepG2 cells were stimulated with ATP. In naive cells, GFP fluorescence was concentrated in the mitochondria and was practically excluded from the nuclear matrix and cytosol even after treatment with ATP, as shown by the presence of small dark areas between the mitochondria (Fig. 4C). A similar cyto *c*-GFP distribution was observed in cells exposed to C2 only. How ever, in cells treated with C2 + ATP, GFP fluorescence was also found in the cytosol and nuclear matrix (Fig. 4C). Notably, C2 + Ca^{2+} signal-induced redistribution of cyto *c*-GFP to the cytosol was attenuated in the presence of CsA (Fig. 4C). These data pro vide evidence for release of cyto *c* from the mitochondria coupled to the rise of $[Ca^{2+}]_m$ and PTP opening.

3.3.4. Simultaneous measurement of Ca^{2+} signal-induced $\Delta\Psi_m$ loss and caspase activation in C2-pre treated intact H9c2 myotubes—Release of cytochrome *c* and other pro-apoptotic factors from mitochondria leads to the activation of effector caspases that execute the final phase of apoptosis. To monitor activation of caspases after $[Ca^{2+}]_m$ rise, we did simultaneous confocal imaging of $\Delta\Psi_m$ and a cell-permeable fluorogenic caspase substrate (PhiPhiLux-G_1D_2). Images of F_{TMRE} show that in response to C2 + caffeine, mitochondrial depolarization occurred in two myotubes (cells A and B), whereas $\Delta\Psi_m$ was not changed in several small cells (e.g. cells C and D) (Fig. 5A). After addition of the caspase substrate, generation of the fluorescent cleavage product was observed in the myotubes displaying mitochondrial depolarization waves (shown in blue in the over lay image; time courses for cells A and B; Fig. 5A), but no change appeared in the non-depolarized cells (e.g. cells C and D; Fig. 5A). Next, we studied whether collapse of $\Delta\Psi_m$ elicited by uncoupler (protonophore) is sufficient to yield rapid cleavage of the caspase substrate (Fig. 5A, second row). Uncoupler caused large decreases in F_{TMRE} in every cell, but the increase in PhiPhiLux fluorescence was almost undetectable. These data suggest that the mitochondrial changes associated with depolarization and Ca^{2+} release waves are effective at initiating caspase activation.

3.3.5. Measurement of Ca^{2+} signal-induced apoptosis in C2-pretreated intact myotubes—To determine whether mitochondrial waves and caspase activation are followed by ordered execution of the apoptotic program, PS expo sure was evaluated by annexin staining (Fig. 5B) and nuclear morphology was studied by labeling with Hoechst 33342 and propidium iodide (Fig. 5C). In myotubes exposed to C2 and subsequently to caffeine, the fraction of cells displaying annexin positivity (Fig. 5B) and nuclear condensation was substantially increased (Fig. 5C). C2 or caffeine treatment by itself failed to exert a similar effect in 6 h (Fig. 5B and C). The effect of C2 + caffeine was attenuated by CsA (Fig. 5B). Thus, execution of the complete apoptotic program was established by the signaling pathway that utilized mitochondrial excitability and intermitochondrial communication to coordinate activation of the mitochondrial phase of apoptosis throughout the cell.

4. Discussion

Apoptosis induced by cytoplasmic calcium signals is commonly mediated through mitochondrial Ca^{2+} transfer and PTP-dependent membrane permeabilization but several alternative mechanisms have also been described including $[Ca^{2+}]_c$-induced (1) activation of calcineurin to dephosphorylate Bad that in turn, translocates to the mitochondria to initiate Bax/Bak-dependent OMM permeabilization [32]; (2) activation of calpain to cleave the endogenous calcineurin inhibitor cain/cabin1 [33]; (3) activation of calpain that cleaves Bid

to form truncated Bid that also initiates the Bax/Bak pathway [34]; (4) activation of calpain that cleaves the Na^+/Ca^{2+} exchanger to cause cytoplasmic Ca^{2+} retention [35]; (5) activation of calpain promotes the internalization of the PMCA to augment cytoplasmic Ca^{2+} retention [36]. The $[Ca^{2+}]_c$ signal also controls the mitochondrial fusion– fission and motility dynamics to modulate the Ca^{2+} transfer to the mitochondria and the execution of apoptosis [37–40]. To evaluate the $[Ca^{2+}]_c$ signal propagation to the mitochondria, simultaneous imaging of $[Ca^{2+}]_c$ and $[Ca^{2+}]_m$ (3.2.1.) is useful. In addition, the sensitivity of the downstream apoptotic markers to inhibitors of the mitochondrial Ca^{2+} uptake, RuRed or Ru360 provides information on the proapoptotic role of the $[Ca^{2+}]_m$ signal. Since RuRed and Ru360 do not permeate the plasma membrane of several cell types [41], in intact cell experiments, the inhibition of mitochondrial Ca^{2+} uptake has to be confirmed or the drug has to be microinjected. To clarify whether PTP opening occurred, demonstration of the dissipation of the $\Delta\Psi_m$ (3.2.2&3.), the delayed $[Ca^{2+}]_c$ dysregulation (3.1., 3.2.1 and 2) and the quench of calcein compartmentalized in the mitochondria [42] is suitable. However, it has to be clarified whether any of these changes or the downstream apoptotic response (3.3.4 and 5) was sensitive to inhibitors of the PTP (e.g. CsA, Me-Val-CsA, sanglifehrin A). Notably, CsA also binds and affects the function of cytoplasmic proteins (e.g. calcineurin), which limits the use of this drug in intact cells. An alternative possibility is to perform studies in cyclophilin $D^{-/-}$ cells or animals that show desensitization of the PTP towards Ca^{2+} [43,44].

Release of IMS proteins that exert pro-apoptotic effects in the cytoplasm couples the execution of apoptosis to the PTP opening. However, the mechanism of OMM permeabilization in the cells remains unclear. In isolated mitochondria, PTP opening show large scale swelling of the matrix, which can cause rupture of the OMM. However, inside the cells, mitochondrial swelling is less because of the presence of membrane impermeant macromolecules in the cytoplasm. In some paradigms, PTP opening results in cyto *c*-GFP release only after recruitment of Bax [45]. Thus, in addition to the swelling induced rupture of the OMM, other mechanisms may also contribute to the OMM permeabilization. Visualization of the release of cyto *c*-GFP (3.2.3 and 3.3.3.) and other fluorescently tagged IMS proteins (e.g. SMAC, AIF) provides some clues to the mechanism of the calcium signal-induced OMM permeabilization [46–48].

Multiple apoptotic pathways converge on effector caspase activation (3.3.4), PS exposure and nuclear condensation/fragmentation (3.3.5). Visualization of these processes is a standard procedure to confirm that the calcium signal-initiated pathway led to the execution of apoptosis. Spatially resolved measurement of the effector caspase activation in intact cells (3.3.4) has revealed that the Ca^{2+}-dependent mitochondrial membrane permeabilization has a local effect on caspase activation, indicating that the microenvironment of the permeabilized mitochondria may offer particularly favorable condition for caspase activation [26]. Since the fluorogenic caspase substrates are not absolutely specific for the caspases, the sensitivity of the fluorescence increase to caspase inhibitors (e.g. zVADfmk) has to be tested.

A striking aspect of the fluorescence imaging approach is the novel information about the subcellular spatial organization of the mitochondrial phase of apoptosis. During the calcium signal-driven apoptosis, some mitochondria serve as pacemakers and initiate regenerative mechanisms of the membrane permeabilization to recruit all the organelles in a coordinated manner (3.2.1–3, 3.3.1 and 4). Visualization of $[Ca^{2+}]_c$ and $[Ca^{2+}]_m$ and pharmacological interventions provided evidence for a Ca^{2+}-dependent coupling between the individual organelles [22,26]. In other paradigms and even in the $[Ca^{2+}]_m$-activated pathway, mitochondria-derived ROS may have significance in the intermitochondrial communication. Visualization of the spatiotemporal pattern of ROS is difficult to discern since the

illuminating light and several fluorescent probes are also source of ROS production. Nevertheless, ROS coupling among the mitochondria has been clearly documented in some cases [24,25]. Several pharmacological inhibitors and genetic approaches (e.g. superoxide dismutase, catalase overexpression and knockout) are also available to clarify the possible involvement of ROS. Since mitochondrial Ca^{2+} uptake can induce ROS formation and Ca^{2+} synergizes with some forms of ROS in the opening of the PTP, Ca^{2+} and ROS effects are often dependent on each other [49].

Calcium signal-induced apoptosis has been show to depend on a local Ca^{2+} transfer between ER/SR and mitochondria in several paradigms [13,21]. As a feedback loop, cytochrome *c* released from the mitochondria and mitochondria-derived ROS may locally pro mote IP3 R/RyR-mediated Ca^{2+} mobilization from the ER [50,51]. In addition, at the sites where the ER is physically bound to the mitochondria (mitochondria associated membranes), lip ids (e.g. sphingolipids) and membrane proteins (e.g. Bcl-2 family proteins) may also transmit signal between the two organelles. Labeling of cells with various combinations of fluorescent dyes and high resolution fluorescence imaging allow measurements of some aspects of the local Ca^{2+} interactions (3.2. and 3.3, [13,52,53]) but Ca^{2+} sensitive fluorescent and lumines cent proteins targeted to different parts of the ER and mitochondria have some clear advantages. These include specific targeting and in some cases, the possibility of ratio metric recording. How ever, the relatively narrow dynamic range and some artifacts (e.g. pH) have to be considered when Ca^{2+}-sensitive fluorescent proteins are used [54,55]. Regardless of the numerous potential problems the presently available probes and fluorescence measurements provide a versatile toolkit for the investigation of calcium signalling in apoptosis.

Acknowledgments

We thank Drs. György Csordás, Gábor Szalai, Pal Pacher, Muniswamy Madesh, and Mrs. Erika Davies for their dedicated efforts in setting up the approaches described here. This work was supported by R01-GM59419 from the National Institutes of Health to G.H.

References

1. Berridge MJ, Bootman MD, Roderick HL. Nat. Rev. Mol. Cell Biol. 2003; 4(7):517–529. [PubMed: 12838335]
2. Rizzuto R, Pozzan T. Physiol. Rev. 2006; 86(1):369–408. [PubMed: 16371601]
3. JW, Putney, Jr; Thomas, AP. Curr. Biol. 2006; 16(18):R812–R815. [PubMed: 16979553]
4. Montero M, et al. Nat. Cell Biol. 2000; 2(2):57–61. [PubMed: 10655583]
5. Joseph SK, Hajnoczky G. Apoptosis. 2007; 12(5):951–968. [PubMed: 17294082]
6. Orrenius S, Zhivotovsky B, Nicotera P. Nat. Rev. Mol. Cell Biol. 2003; 4(7):552–565. [PubMed: 12838338]
7. Bernardi P. Physiol. Rev. 1999; 79(4):1127–1155. [PubMed: 10508231]
8. Green DR, Kroemer G. Science. 2004; 305(5684):626–629. [PubMed: 15286356]
9. Kim JS, He L, Lemasters JJ. Biochem. Bio phys. Res. Commun. 2003; 304(3):463–470.
10. Kroemer G, Galluzzi L, Brenner C. Physiol. Rev. 2007; 87(1):99–163. [PubMed: 17237344]
11. Wang X. Genes. Dev. 2001; 15(22):2922–2933. [PubMed: 11711427]
12. Bernardi P, Forte M. Novartis Found. Symp. 2007; 287:157–164. [PubMed: 18074637]
13. Szalai G, Krishnamurthy R, Hajnoczky G. EMBO. J. 1999; 18(22):6349–6361. [PubMed: 10562547]
14. Scorrano L, et al. J. Biol. Chem. 2001; 276(15):12035–12040. [PubMed: 11134037]
15. Jacobson J, Duchen MR. J. Cell Sci. 115. 2002; (Pt 6):1175–1188.
16. Hajnoczky G, Davies E, Madesh M. Biochem. Biophys. Res. Commun. 2003; 304(3):445–454. [PubMed: 12729578]
17. Gerasimenko JV, et al. J. Cell Sci. 2002; 115(Pt 3):485–497. [PubMed: 11861756]

18. Pinton P, et al. EMBO J. 2001; 20(11):2690–2701. [PubMed: 11387204]
19. Tang TS, et al. Proc. Natl. Acad. Sci. USA. 2005; 102(7):2602–2607. [PubMed: 15695335]
20. Nicholls DG, et al. J. Neurosci. Res. 2007; 85(15):3206–3212. [PubMed: 17455297]
21. Csordas G, et al. J. Cell Biol. 2006; 174(7):915–921. [PubMed: 16982799]
22. Ichas F, Jouaville LS, Mazat JP. Cell. 1997; 89(7):1145–1153. [PubMed: 9215636]
23. Hajnoczky G, Pacher P, Lin X. IUBMB Life. 2001; 52(3–5):237–245. [PubMed: 11798038]
24. Zorov DB, et al. J. Exp. Med. 2000; 192(7):1001–1014. [PubMed: 11015441]
25. Aon MA, et al. J. Biol. Chem. 2003; 278(45):44735–44744. [PubMed: 12930841]
26. Pacher P, Hajnoczky G. EMBO J. 2001; 20(15):4107–4121. [PubMed: 11483514]
27. Porcelli AM, et al. Methods Cell Biol. 2001; 65:353–380. [PubMed: 11381603]
28. Galluzzi L, et al. Apoptosis. 2007; 12(5):803–813. [PubMed: 17294081]
29. Heiskanen KM, et al. J. Biol. Chem. 1999; 274(9):5654–5658. [PubMed: 10026183]
30. Szalai G, et al. J. Biol. Chem. 2000; 275(20):15305–15313. [PubMed: 10809765]
31. Csordas G, Hajnoczky G. Cell Calcium. 2001; 29(4):249–262. [PubMed: 11243933]
32. Wang HG, et al. Science. 1999; 284(5412):339–343. [PubMed: 10195903]
33. Kim MJ, et al. Proc. Natl. Acad. Sci. USA. 2002; 99(15):9870–9875. [PubMed: 12114545]
34. Chen M, et al. J. Biol. Chem. 2001; 276(33):30724–30728. [PubMed: 11404357]
35. Bano D, et al. Cell. 2005; 120(2):275–285. [PubMed: 15680332]
36. Pottorf WJ 2nd, et al. J. Neurochem. 2006; 98(5):1646–1656. [PubMed: 16923173]
37. Rintoul GL, et al. J. Neurosci. 2003; 23(21):7881–7888. [PubMed: 12944518]
38. Cribbs JT, Strack S. EMBO Rep. 2007; 8(10):939–944. [PubMed: 17721437]
39. Yi M, Weaver D, Hajnoczky G. J. Cell. Biol. 2004; 167(4):661–672. [PubMed: 15545319]
40. Szabadkai G, et al. Mol. Cell. 2004; 16(1):59–68. [PubMed: 15469822]
41. Hajnoczky G, et al. Cell Calcium. 2006; 40(5–6):553–560. [PubMed: 17074387]
42. Petronilli V, et al. Biophys. J. 1999; 76(2):725–734. [PubMed: 9929477]
43. Basso E, et al. J. Biol. Chem. 2005; 280(19):18558–18561. [PubMed: 15792954]
44. Baines CP, et al. Nature. 2005; 434(7033):658–662. [PubMed: 15800627]
45. De Giorgi F, et al. FASEB J. 2002; 16(6):607–609. [PubMed: 11919169]
46. Rehm M, Dussmann H, Prehn JH. J. Cell Biol. 2003; 162(6):1031–1043. [PubMed: 12975347]
47. Arnoult D, et al. EMBO J. 2003; 22(17):4385–4399. [PubMed: 12941691]
48. Loeffler M, et al. FASEB J. 2001; 15(3):758–767. [PubMed: 11259394]
49. Brookes PS, et al. Am. J. Physiol. Cell Physiol. 2004; 287(4):C817–C833. [PubMed: 15355853]
50. Boehning D, et al. Nat. Cell Biol. 2003; 5(12):1051–1061. [PubMed: 14608362]
51. Redondo PC, et al. Biochem. Pharma col. 2004; 67(6):1065–1076.
52. Pacher P, Thomas AP, Hajnoczky G. Proc. Natl. Acad. Sci. USA. 2002; 99(4):2380–2385. [PubMed: 11854531]
53. Hajnoczky G, Hager R, Thomas AP. J. Biol. Chem. 1999; 274(20):14157–14162. [PubMed: 10318833]
54. Palmer AE, Tsien RY. Nat. Protoc. 2006; 1(3):1057–1065. [PubMed: 17406387]
55. Demaurex N. Cell Calcium. 2005; 38(3–4):213–222. [PubMed: 16122797]

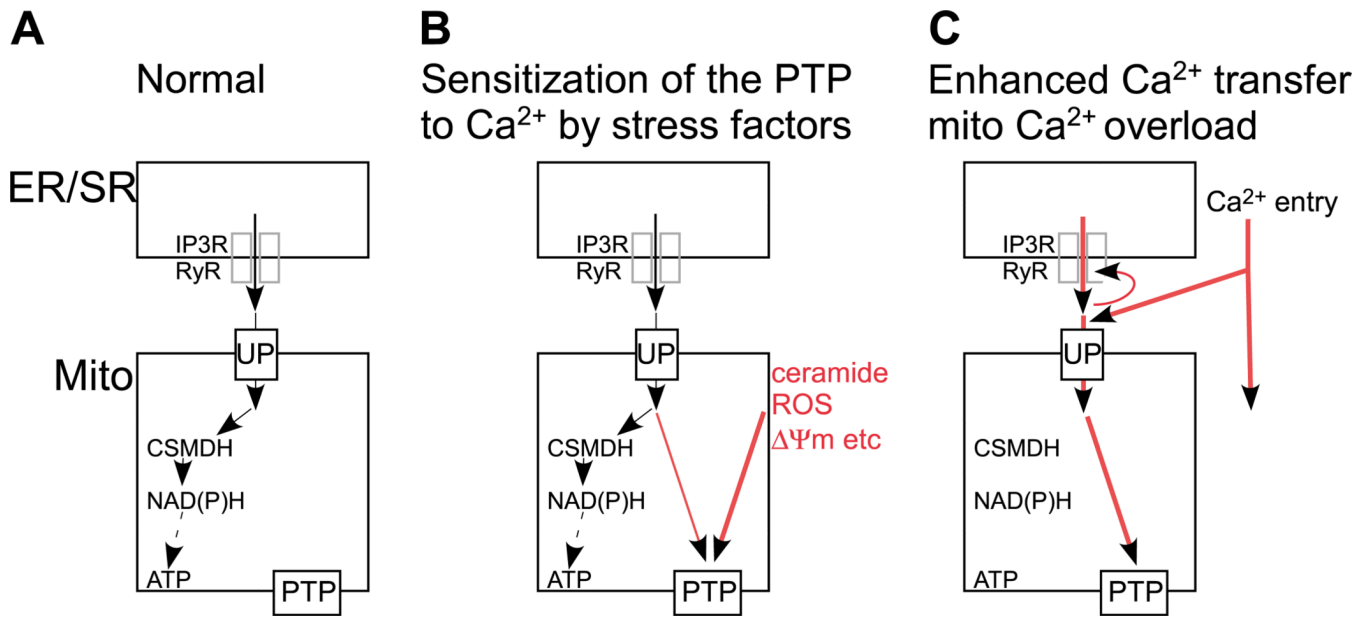

Fig. 1.

Schematic representation of the ER/SR-mitochondrial Ca^{2+} transfer and the intramitochondrial control of energy metabolism and PTP opening by Ca^{2+} under different conditions: (A) Normal, calcium oscillations activate the Ca^{2+}-sensitive mitochondrial dehydrogenases (CSMDH) to enhance ATP production; (B) Mitochondria are exposed to factors that increase the sensitivity of the PTP towards Ca^{2+}; (C) Increased mitochondrial Ca^{2+} transfer leads to PTP opening during physiological calcium oscillations. UP—mitochondrial Ca^{2+} uniporter.

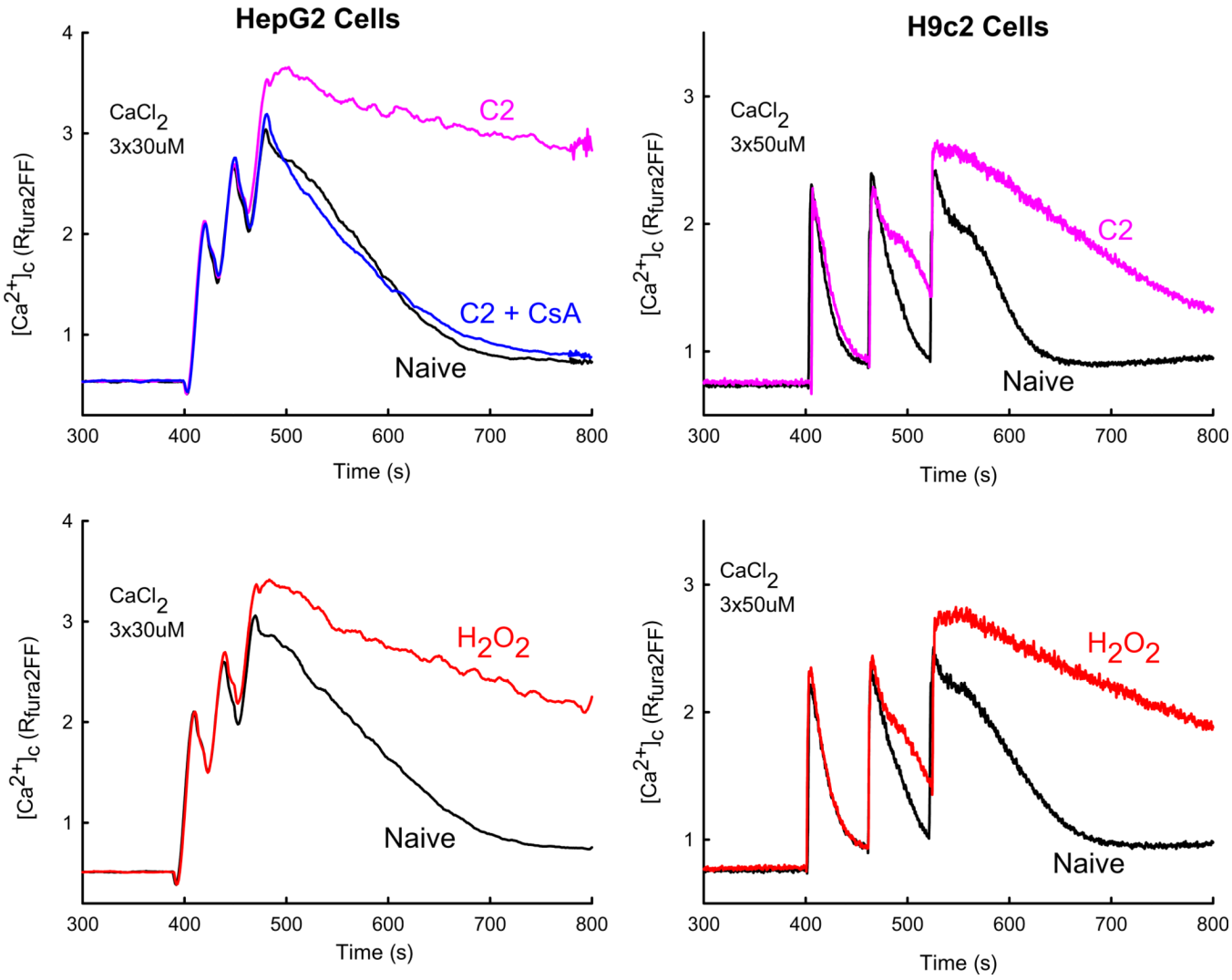

Fig. 2.

PTP opening-dependent delayed $[Ca^{2+}]_c$ dysregulation in suspensions of permeabilized cells.: $[Ca^{2+}]_c$ was measured using fura2FF/FA in suspensions of permeabilized HepG2 (left) and H9c2 (right) cells exposed to pro-apoptotic stimuli. C2 (40 μM, purple), H_2O_2 (50/200 μM, red) or solvent (black) were added 180 s before Ca^{2+} pulsing. The measurements were repeated in the presence of CsA (5 uM, blue). Traces are shown from separate incubations using the same cell preparation.

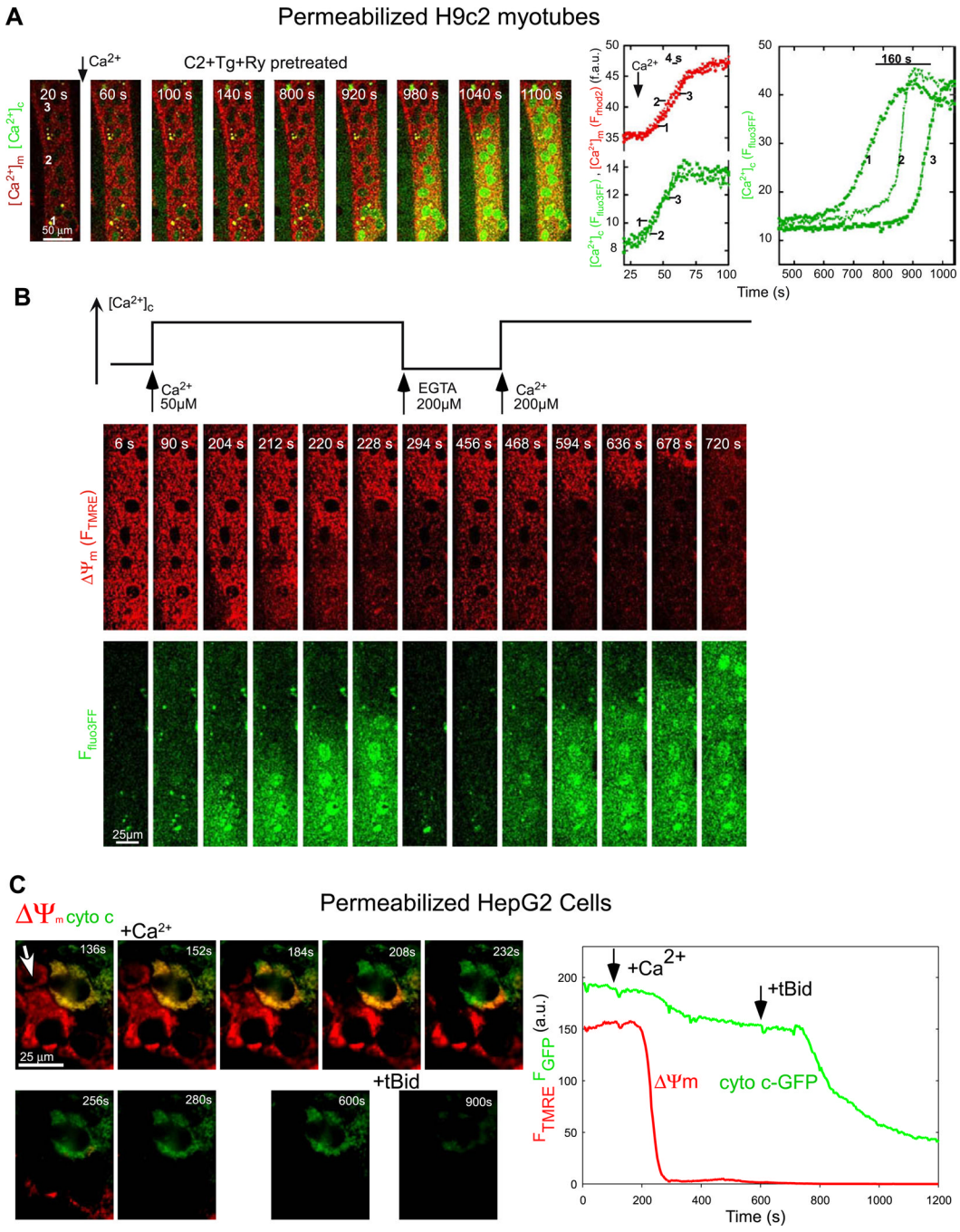

Fig. 3.

Real-time imaging of $[Ca^{2+}]_c$, $[Ca^{2+}]_m$, $\Delta\Psi_m$ and cyto *c*-GFP distribution in permeabilized single cells: (A) Delayed $[Ca^{2+}]_c$ dysregulation in a permeabilized H9c2 myotube pretreated with Tg (2 µM)+ Ry + C2. Simultaneous time-lapse confocal imaging of $[Ca^{2+}]_c$ (green) and $[Ca^{2+}]_m$ (red) was carried out using fluo3FF and compartmentalized rhod2 as described in methods section. Addition of Ca^{2+} (50 µM $CaCl_2$) evoked a delayed and slowly propagating large amplitude $[Ca^{2+}]_c$ wave. The right graph shows time courses (green) calculated for the marked subcellular regions. (B) Dependence of the mitochondrial depolarization and Ca^{2+} release waves on the $[Ca^{2+}]_c$ rise and mitochondrial Ca^{2+} uptake. Simultaneous confocal imaging of $[Ca^{2+}]_c$ and $\Delta\Psi_m$ was carried out in permeabilized H9c2 myotubes. The

fluorescence intensities of TMRE and fluo3FF reflecting $\Delta\Psi_m$ and $[Ca^{2+}]_c$ are depicted on linear red and green scales, respectively. The fluo3FF confocal images reflect $[Ca^{2+}]_c$ changes in the selected focus plane. Therefore, rapid Ca^{2+} mobilization from intracellular stores is associated with fluo3FF responses even if a global $[Ca^{2+}]_c$ rise does not occur. The plot above the confocal image time series shows the time course profile of global $[Ca^{2+}]$ changes in the cytosolic buffer. Waves were elicited in C2-treated permeabilized cells by addition of 50 μM $CaCl_2$ and subsequently stopped by addition of a Ca^{2+} chelator (200 μM EGTA). When global $[Ca^{2+}]_c$ was increased again, propagation of the waves continued the original spatial pattern. Changes in pH in the incubation medium associated with addition of EGTA and Ca^{2+} were <0.1 units. (C) Temporal and spatial organization of mitochondrial depolarization and cyto *c*-GFP release induced by C2+Ca^{2+}. $\Delta\Psi_m$ was monitored simultaneously with cyto *c* distribution in a cyto *c*-GFP-expressing and TMRE-loaded HepG2 cell. Sequential fluorescence images are shown as green ($F_{cytoc\text{-}GFP}$), red (F_{TMRE}) overlays. Depolarization appears as a loss of the red fluorescence, whereas cyto *c*-GFP release appears as a loss of the green fluorescence. Cyto *c*-GFP was expressed only in the cell that is shown in the upper right quadrant. Permeabilized cells were pretreated with C2 (40 μM for 5 min) before addition of Ca^{2+} (50 μM $CaCl_2$) and, subsequently, tBid (25 nM). The Ca^{2+}-induced mitochondrial depolarization started in a discrete subcellular region and propagated as a wave through the cell (direction of the wave is marked by the white arrow in the upper left image). Time course of the fluorescence changes is plotted in the graph. Panels A,B are reproduced with modification from [26], and C is from [16] by permission.

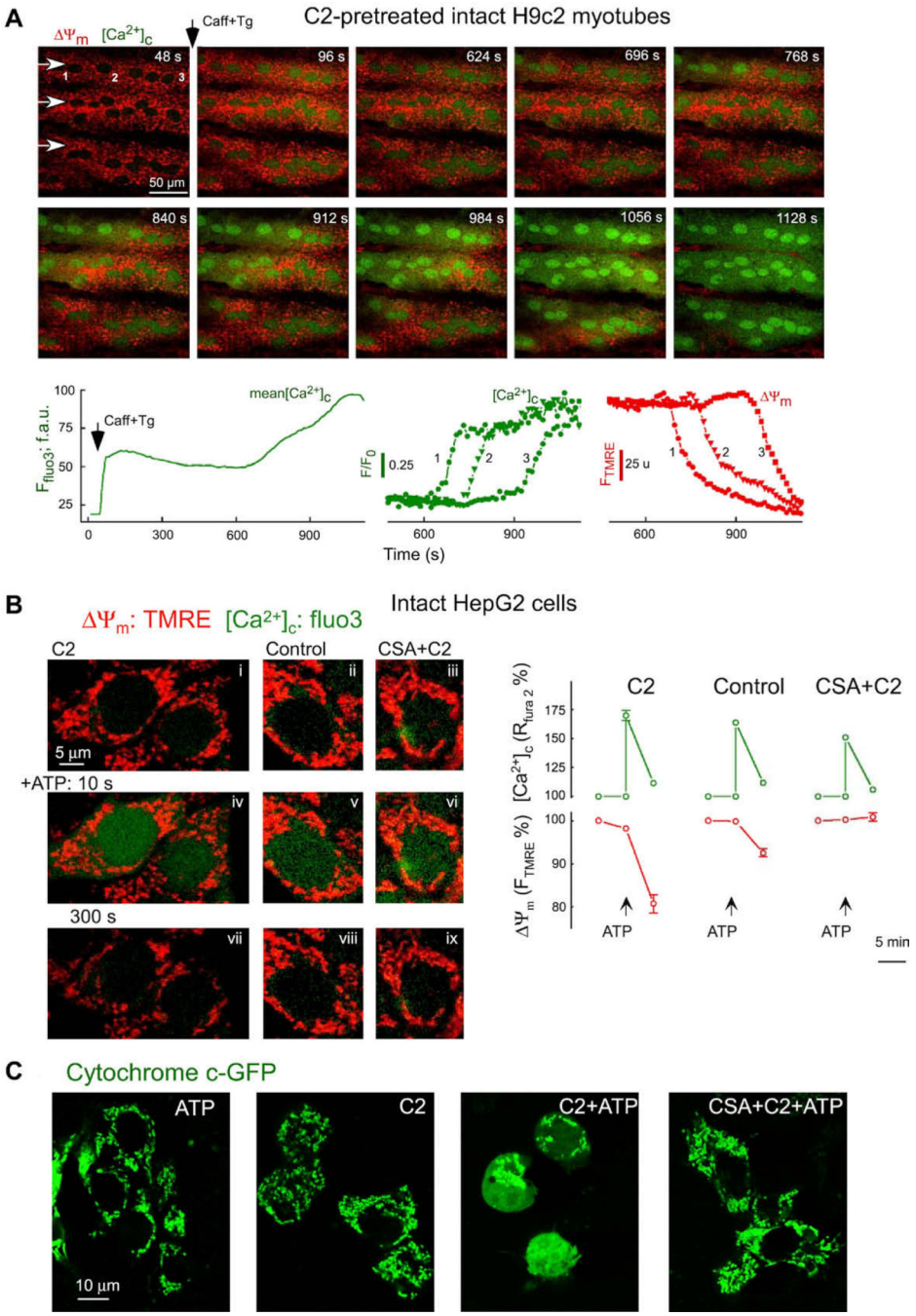

Fig. 4.

Real-time imaging of $[Ca^{2+}]_c$, $\Delta\Psi_m$ and cyto *c*-GFP distribution in intact single cells: (A) RyR-dependent Ca^{2+} release-induced delayed $[Ca^{2+}]_c$ and $\Delta\Psi_m$ dysregulation in intact myotubes. Simultaneous confocal imaging of $[Ca^{2+}]_c$ and $\Delta\Psi_m$ was carried out in intact H9c2 myotubes. Fluorescence intensities of TMRE and fluo3 reflecting $\Delta\Psi_m$ and $[Ca^{2+}]_c$ are depicted on linear red and green scales, respectively. C2-pretreated cells (40 μM for 5 h) were stimulated by addition of caffeine (15 mM) and Tg (2 μM). Arrows in the top left panel show the direction of wave propagation. The graphs show the mean time course profile of $[Ca^{2+}]_c$ for the total area of the upper myotube (left) and time courses of $[Ca^{2+}]_c$ (middle) and $\Delta\Psi_m$ (right) at three intracellular regions selected along the path of wave propagation

(marked with numbers). (B) Activation of the PTP in intact HepG2 cells stimulated with IP_3-linked stimuli. Simultaneous measurements of $[Ca^{2+}]_c$ and $\Delta\Psi_m$ carried out in intact HepG2 cells exposed to C2 (40 μM), solvent or CsA (1 μM) + C2. Confocal images of cells loaded with fluo3 and TMRE showing $[Ca^{2+}]_c$ (green) and $\Delta\Psi_m$ (red) in C2-treated cells (left side), in naive cells (middle) and in CsA + C2-treated cells (right side) before addition of 200 μM ATP (images i–iii), at 10 s (iv–vi) and at 300 s (vii–ix) after stimulation. Graphs show the comparison of $[Ca^{2+}]_c$ increases and mitochondrial depolarizations measured in each condition at the peak of the $[Ca^{2+}]_c$ rise and at 300 s stimulation. Data are normalized to prestimulation values. (C) Redistribution of cyto *c*-GFP in intact HepG2 cells stimulated with C2 and IP_3-linked stimuli. HepG2 cells were transfected using cyto *c*-GFP plasmids. Confocal images show distribution of cyto *c*-GFP in cells exposed to ATP (100 μM) alone, C2 (40 μM) alone, ATP+C2 or CsA (1 μM)+ATP+C2 for 6 h. Panels A is reproduced from [26], B is from [13] and C is from [16] by permission.

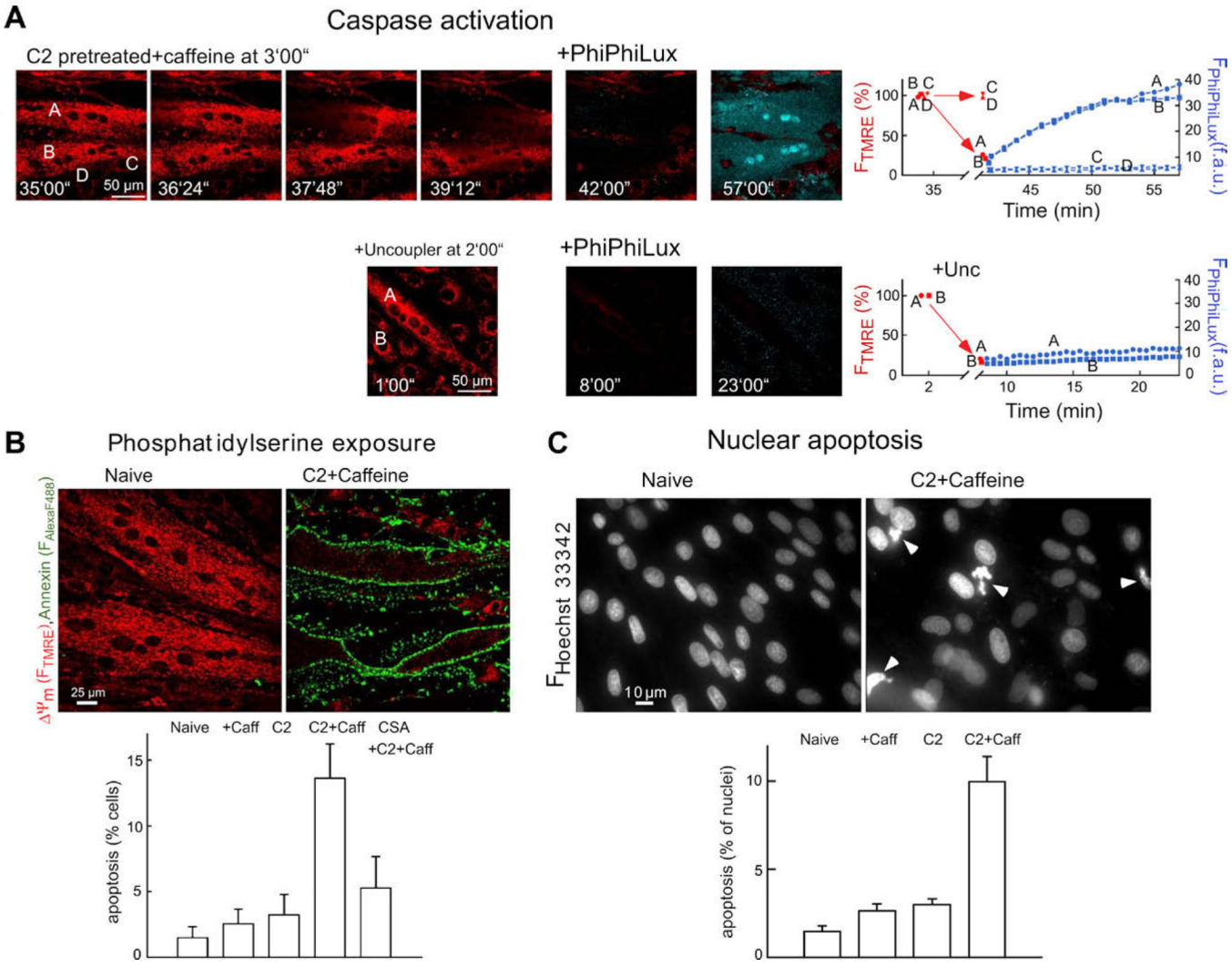

Fig. 5.

Fluorescence imaging of caspase activation and apoptosis in intact H9c2 myotubes: (A) Simultaneous confocal imaging of $\Delta\Psi_m$ and fluorescent caspase cleavage products in single intact H9c2 myotubes. Cells were treated with C2 (40 µM for 5 h) followed by caffeine (15 mM) and Tg (2 µM) additions. After the Ca^{2+} signal-induced depolarization wave or the uncoupler (FCCP 5 µM + oligomycin 10 µg/ml)-induced depolarization was completed, the buffer was replaced with RPMI containing 5 µM cell-permeable fluorogenic caspase substrate (+ PhiPhiLux). Overlaid images of F_{TMRE} (red) and $F_{PhiPhiLux}$ (blue) are shown. Time course for $\Delta\Psi_m$ (red) and fluorescent caspase cleavage products (blue) is shown in the graphs. (B) PS exposure as visualized by annexin–Alexa Fluor 488 staining of intact myotubes. The adherent myotubes were pre-incubated with C2 (40 µM) or C2 + CsA (1 µM) or solvent for 2 h and, subsequently, 15 mM caffeine or solvent was also added for 4 h. Note that $\Delta\Psi_m$ was measured simultaneously by annexin staining using TMRE. In myotubes with annexin–Alexa Fluor 488 staining, F_{TMRE} was very low, indicating large mitochondrial depolarization. PS positive cells were plotted as % of total cell number in the graph (mean ± SE). (C) Nuclear apoptosis visualized by staining with Hoechst 33342/propidium iodide. Cells were treated as described in (B). Propidium iodide was excluded from >99% of naive, C2-treated and caffeine-stimulated cells and >98% of the C2 + caffeine treated myotubes,

indicating the absence of late apoptotic or necrotic cells. Number of fragmented/condensed nuclei are shown in the graph (mean ± SE). Figure is reproduced from [26].

Table 1

Fluorophores and fluorescent proteins used in the present measurement.

Probes	Primary location	Excitation (nm)	Emission (nm)	Measurements
Fura2 (Teflabs)	Cytoplasm	340/380	≥500	$[Ca^{2+}]_c$
Fura2FF (Teflabs)	Cytoplasm	340/380	≥500	$[Ca^{2+}]_{c,}$ supramicromolar
Fluo3	Cytoplasm	488	530	$[Ca^{2+}]_c$
Fluo3FF	Cytoplasm	488	530	$[Ca^{2+}]_{c,}$ supramicromolar
Rhod2	Mt matrix	568	≥580	$[Ca^{2+}]_m$
Rhod2FF	Mt matrix	568	≥580	$[Ca^{2+}]_{m,}$ supramicromolar
TMRE	Mt matrix	545	≥580	$\Delta\Psi_m$
JC1	Mt matrix, cytoplasm	490/570	535/595	$\Delta\Psi_m$
Cyto *c*-GFP	IMS	490	530	Cyto *c* release
PhiPhiLux-G_1D_2 (Alexis)	Cytoplasm	488	530	Effector caspase activity
Rhodamine 110, bis-(L-aspartic acid amide), trifluoroacetic acid	Cytoplasm	488	520	Effector caspase activity
Annexin–Alexa Fluor 488	Plasma membrane	488	530	PS in apoptotic cells
Propidium iodide	Nuclear DNA	545	580	Condensed and fragmented nuclei
Hoechst 33342	Nuclear DNA	340	460	Condensed and fragmented nuclei

Table 2

Instrumentation.

Technique	Excitatin light source	Excitation wave-length selection	Emission wavelength selection	Detection
Fluorometry (PTI Delta RAM)	Xe continuous 300–600 nm	Monochromator	Monochromator	Photomultiplier
Fluorescence imaging (custom designed)	Xe continuous	Monochromator (PTI) Excitation filters (Lambda DG, Sutter or filter wheel, ASI)	Emission filters (filter wheel)	CCD camera (PXL, Photometrics or Pluto, Pixelvision)
Confocal imaging (BioRad Radiance 2002)	Laser: 442 nm HeCd, 488 nm KrAr, 568 nm KrAr and 635 nm red diode	na	Emission filters (filter wheel)	Photomultiplier